Molecule Detection with Graphene Dimer Nanoantennas

François Aguillon, Dana Codruta Marinica, Andrey Borissov

Molecule detection with graphene dimer nanoantenna

François Aguillon, Dana Codruta Marinica, and Andrei G. Borisov*

Institut des Sciences Moléculaires d'Orsay, UMR 8214, CNRS, Université Peris-Saclay, Bâtiment 520, 91405 Orsay Cedex, France

E-mail: andrei.borissov@u-psud.fr

Phone: +33 (0)1 69157697

Abstract

Using the tight binding description of the electronic structure of graphene and a time-dependent quantum approach we address the vibrational excitation of molecules in the near field of a graphene nanoantenna. The possibility to tune the graphene plasmon frequency by electrostatic doping allows an efficient resonant excitation of the infra-red (IR) active vibrational modes via the coupling between molecular dipole and plasmon near field. We show that for the carbon monoxide CO molecules placed in the gap of a dimer antenna formed by the 20 nm size graphene patches, an excitation of the $v = 1 \leftarrow 0$ transition leads to a distinct molecular signature in the IR absorption spectrum of the system. A very small number of molecules down to a single molecule placed in the antenna gap can thus be detected. Along with IR active vibrations, the inhomogeneity of the plasmonic near field allows vibrational excitation of IR inactive molecules via molecular quadrupole. The resonant excitation of the N_2 molecule vibration is thus observed in the calculated absorption spectra, albeit the molecule signature is essentially smaller than for the CO molecule. Obtained with molecules described on the ab initio

quantum chemistry level, our results provide quantitative insights into the performance of graphene nanoflakes and their dimers for molecular sensing.

Introduction

The possibility to engineer the enhanced optical fields at the spatial scales well below that of the wavelength, as offered by plasmonic structures, allows one to control the light matter interaction at the nanometer (nm) scale with numerous applications for nonlinear optics,[1] optoelectronics,[2] and single molecule sensing[3–6] among others. For quantum emitters, the exciton coupling with plasmon modes of the nanoantenna determines the dynamics of the excitation and decay, as well as the far field emission,[7–12] with the possibility of detecting a single quantum emitter.[3,13–15] In this respect, the localization of plasmonic fields by atomic-scale protrusions in plasmonic cavities[16–18] provides a spectacular sub-molecular resolution in the observation of the single-molecule luminescence maps,[19–25] maps of the Lamb shift of the excitation energy,[26] and Raman maps of molecular vibrations.[27–30] In these experiments, the energy is resonantly exchanged between the plasmon mode and the electronic transitions in individual nanoobject placed in the junction, with further excited state evolution involving e.g. vibrational excitation. It is worth noting that in a broader context, the strong coupling between molecular vibrations and optical modes of the nanocavity leads to e.g. exciting possibilities of polaritonic chemistry.[31–33]

Recently the 2D materials emerged as promising platforms for electrical[34–36] and optical[37–39] detection up to the single molecule limit. In the case of optical detection, the low energy optical phonons or plasmons of the 2D materials can resonantly couple to molecular vibrations greatly improving the sensitivity of surface-enhanced infrared adsorption spectroscopy (SEIRA). In particular, for graphene nanostructures, the energies of the plasmon modes can be tuned by charge doping with e.g. an applied bias, leading to versatile, tunable, broad frequency range sensors. Several groups reported detection and identification of

molecules adsorbed at low concentrations on graphene ribbons.[40–46] As well, the possibility of molecular detection exploiting the change of the linear and, in particular, of the nonlinear response of Gr nanoislands upon molecular adsorption has been theoretically addressed.[47–50]

In this work we change the paradigm, and instead of considering a layer of molecules adsorbed on top of a graphene nanoobject, we theoretically address the possibility to detect small amounts of molecules with the ultimate limit of a single molecule placed in the nanometer size gap of graphene dimer nanoantenna. Indeed, as known from the 3D metal plasmonics, shrinking an effective plasmon mode volume in the plasmonic nanogap configuration leads to a strong increase of the plasmon-exciton interaction.[12,51–58] We show that this also holds in 2D for the narrow junction between graphene patches with possibility of the detection of single CO molecules via plasmon coupling to molecular vibration. We analyze how the molecule induced features in the absorption spectra depend on molecular orientation, on the number of the molecules located in the gap region, and on the damping of molecular vibrations. Along with an excitation of the infra red (IR) active vibrational modes via dipolar coupling, the inhomogeneity of plasmonic near fields allows vibrational excitation of molecules via quadrupolar coupling. With an example of N_2 molecule interacting with graphene nanoantenna we provide a quantitative analysis of this mechanism leading to the weak signatures of molecular vibrational excitation in the IR absorption spectra.

Unless otherwise stated atomic units are used throughout the paper.

Optical response of the graphene nanoantenna

We start with the analysis of the optical response of individual graphene nanoantennas necessary to understand the changes introduced by analyte molecules. Owing to the strong enhancement of the incident electromagnetic field in the gap between the nanoparticles,[59] the metal dimer geometry has proven its efficiency in enhancing the coupling between plasmons and electronic excitations.[8,10,55–58] Thus, in quest of enhanced plasmon interaction

with molecular vibration for SEIRA we consider graphene antennas formed by nanoflakes of circular and triangular shapes and by their dimers as depicted in Fig. 1. The nanostructures are cut from an ideal graphene plane, and the carbon atoms with a single neighbor are removed at the borders. The gap width of the dimer antennas is $h = 2$ nm. The single circular nanoparticle of radius $R_{cl} = 10.6$ nm comprises $N_C = 13452$ carbon atoms, and the equilateral triangle shape nanoparticle with armchair edges and side length $L = 28.5$ nm comprises $N_C = 13458$ carbon atoms. The apexes of the triangle are set smooth with a curvature radius $r_a = 1$ nm. We use the coordinate system with z-axis perpendicular to graphene plane and in-plane y and x axes. The x-axis is set along the dimer axis.

The optical response of the nanoantenna is calculated in real time using the quantum time-dependent tight binding (TDTB) description of the electron density dynamics triggered in graphene by an external perturbation. Our method is based on the quantum approach to graphene plasmonics developed by García de Abajo and collaborators[60,61] considering the nonretarded description of potentials. This approximation is fully justified here since the size of the graphene nanoantennas is two orders of magnitude smaller than the wavelength of the radiation resonant with molecular vibrations. For further details on the method we refer the interested reader to the Supporting Information (SI).

For each nanoantenna geometry, the near field and induced charge density calculated with TDTB for the plasmon modes of dipolar character relevant for the present study are shown in Fig. 1. The nanoantennas are excited by the linearly x-polarized plane wave resonant with dipole plasmon (DP) of the single-particle antenna and bonding dipole plasmon (BDP) of the dimer. The graphene nanoparticles are electronically doped to a Fermi energy $E_F = 0.36$ eV as measured from the neutrality (Dirac) point. In practice, the relative number of extra-electrons added to each nanoparticle Q_e/N_C (Q_e is the electronic charge) equals to 3.4×10^{-3} for the circular geometry, and 5.6×10^{-3} for triangular geometry resulting in plasmon frequencies $\omega_{\mathrm{DP}}^{\bigcirc} = 0.284$ eV, $\omega_{\mathrm{DP}}^{\triangle} = 0.262$ eV, $\omega_{\mathrm{BDP}}^{\bigcirc\bigcirc} = 0.267$ eV, and $\omega_{\mathrm{BDP}}^{\triangle\triangle} = 0.250$ eV. In line with previous theoretical studies on conventional metal[62–65] and graphene

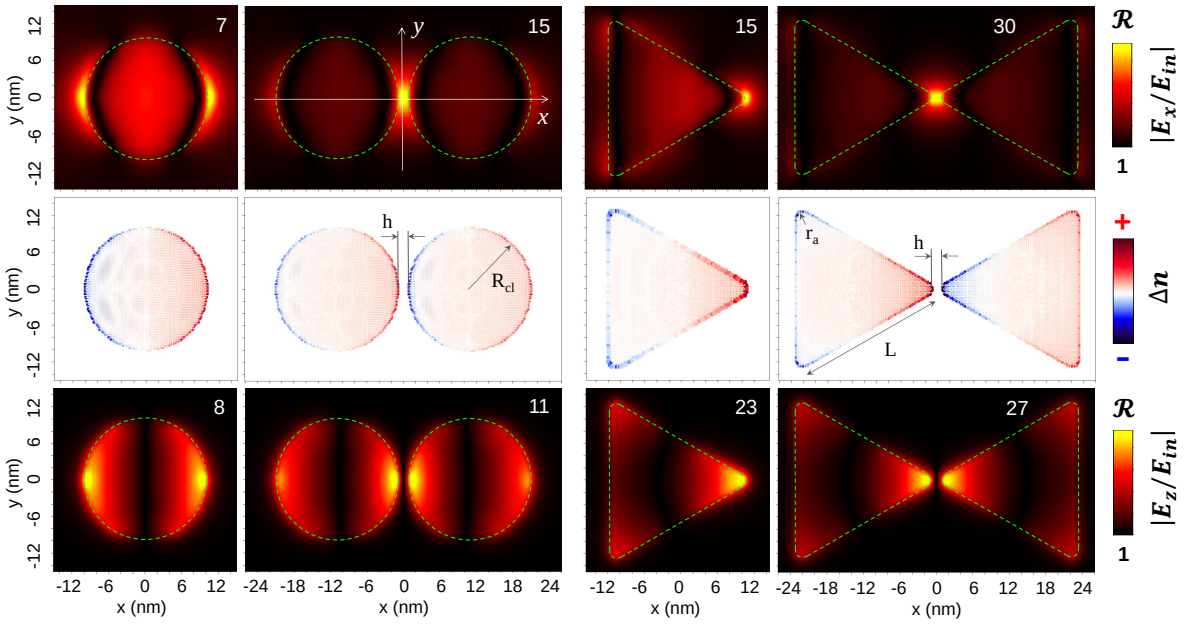

Figure 1: Geometry of the studied dimer antennas together with spatial maps of the charge densities (middle row panels) and the absolute value of the x- (E_x, top row panels) and z-components (E_z, bottom row panels) of the near fields measured in the $(x, y, z = 1)$ nm- plane above the graphene surface. The plasmonic gap $h = 2$ nm, $R_{cl} = 10.6$ nm, $L = 28.5$ nm, and $r_a = 1$ nm. We use the coordinate system with z-axis perpendicular to graphene plane and in-plane y and x axes. For the dimer, the origin of coordinates is set at the middle of the gap. The nanoantennas are excited by an incident x-polarized plane wave resonant with dipolar plasmon in the case of the individual nanoparticle and with the bonding dipolar plasmon in the case of the dimer. The near field is normalized to the amplitude of the incident plane wave $E_{\rm IR}$ so that the upper and lower row panels show the enhancement ($\mathcal{R}_x$ and $\mathcal{R}_z$) of the corresponding components of the near field. The maximum value of $\mathcal{R}$ is indicated with a white number on each panel. The graphene nanoparticles are electronically doped to a Fermi energy $E_F = 0.36$ eV The color code is explained in the inserts.

plasmonic dimers[66–68] our results demonstrate that, as compared to the single graphene nanoantenna, the dimer geometry allows to reach much stronger near field in the gap region. For the x-component of the induced field, the maximum field enhancement is produced in the nanoantenna gap by the concentration of the plasmonic charges of opposite sign induced at graphene surfaces across the junction. By symmetry, the z -component of the induced field is zero at the middle of the gap. It reaches a maximum above the graphene edges facing the gap because of the strongest concentration of plasmonic charges. Comparing the two dimer geometries, the bowtie antenna leads to the most efficient field enhancement owing to

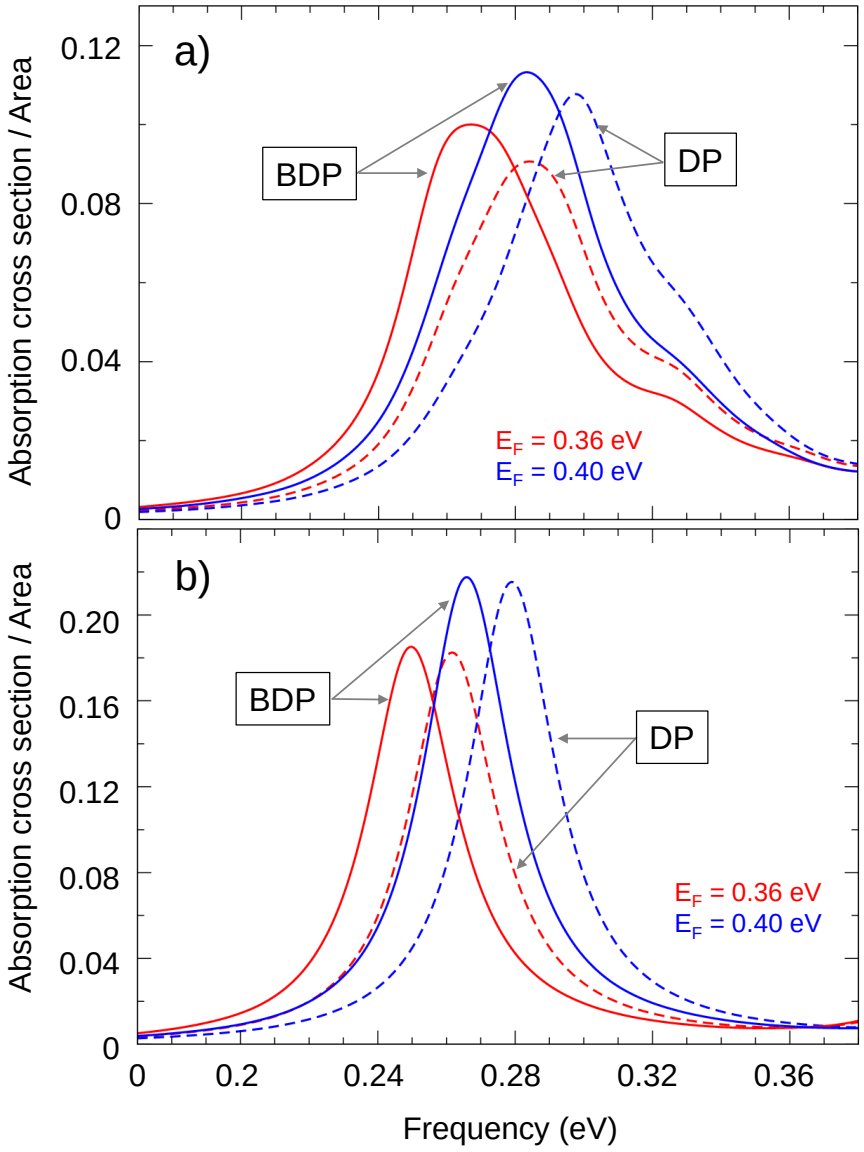

Figure 2: Absorption spectra for the monomer (dashed lines) and dimer (solid lines) graphene antennas of circular (panel a) and triangular (panel b) geometry. The absorption cross section σ normalized per geometric area of the nanoantenna is shown as function of the frequency of the electromagnetic x-polarized incident plane wave. For each geometry, the TDTB calculations are performed for two different energies of the Fermi level, E_F, as explained in the inserts of each panel. DP stands for the dipolar plasmon of the single nanoflake antenna, and BDP stands for the bonding dipole plasmon of the dimer.

the lightning rod effect. However, the stronger near fields are localized in this case within a much narrower spatial region as compared to the dimer of circular nanoparticles. This is

certainly a limitation considering the "active" antenna area for efficient molecule detection.

The characterization of the optical properties of the nanoantennas is continued in Fig. 2. The optical absorption spectra calculated with TDTB for the monomer and dimer antennas of circular and triangular geometry are shown for two different levels of electronic doping characterised by the Fermi energies $E_F = 0.36$ eV, and $E_F = 0.4$ eV illustrating the tunability of the optical response. Within the frequency range of interest, each absorption spectrum is dominated by the well-defined plasmon resonance. The dipolar character of the underlying plasmon modes follows from the maps of the induced densities and near fields (see typical examples in Fig. 1). The calculated resonance energies and widths are summarized in Table 1. Similar to the previous studies, we also obtained that the plasmon decay via nanoparticle edge effects strongly depends on the nanoflake geometry[60,69] (see further discussion in SI). Interestingly, for the bowtie and single triangle antenna with armchair edges the plasmon modes are better defined as compared to the circular geometry used here. The narrower width of the resonances indicates in this case smaller edge effects.

Table 1: Resonance frequencies and widths of the plasmon modes of dipolar character: dipole plasmon (DP) for single particle antenna (Monomer), bonding dipole plasmon (DP) for plasmonic dimer (Dimer), All quantities are given in [eV].

$E_F = 0.36$		$E_F = 0.40$	
$\omega_{\mathrm{DP}}^{\bigcirc} = 0.284$	$\Gamma_{\mathrm{DP}}^{\bigcirc} = 0.058$	$\omega_{\mathrm{DP}}^{\bigcirc} = 0.298$	$\Gamma_{\mathrm{DP}}^{\bigcirc} = 0.063$
$\omega_{\mathrm{BDP}}^{\bigcirc\bigcirc} = 0.267$	$\Gamma_{\mathrm{BDP}}^{\bigcirc\bigcirc} = 0.055$	$\omega_{\mathrm{BDP}}^{\bigcirc\bigcirc} = 0.283$	$\Gamma_{\mathrm{BDP}}^{\bigcirc\bigcirc} = 0.057$
$\omega_{\mathrm{DP}}^{\triangle} = 0.262$	$\Gamma_{\mathrm{DP}}^{\triangle} = 0.032$	$\omega_{\mathrm{DP}}^{\triangle} = 0.279$	$\Gamma_{\mathrm{DP}}^{\triangle} = 0.032$
$\omega_{\mathrm{BDP}}^{\triangle\triangle} = 0.250$	$\Gamma_{\mathrm{BDP}}^{\triangle\triangle} = 0.032$	$\omega_{\mathrm{BDP}}^{\triangle\triangle} = 0.266$	$\Gamma_{\mathrm{BDP}}^{\triangle\triangle} = 0.032$

For a given nanoantenna, with increasing E_F the plasmon resonance shifts to higher energy as consequence of the higher electronic density in the graphene π-band. Indeed, considering the Drude-like in-plane conductivity $\sigma_{\rm Gr} = \frac{E_F}{\pi} \frac{i}{\omega + i\gamma/2}$ one obtains the dispersion relation of surface graphene plasmons $\omega_{\rm sp} \propto \sqrt{E_F}$.[70,71] The absorption cross sections normalised to the antenna area are very similar for the dimer and monomer antennas formed by nanoflakes of identical shape. At the same time, for a fixed E_F, the dimer geometry leads to a notable redshift of the plasmon mode of dipolar character because of the attractive Coulomb interaction between the plasmonic charges of opposite sign across the junction.[59,67]

Considering the finite resonance width and the tunability of the resonance frequency with electronic doping (E_F), the resonant optical response of the nanoantennas covers the energy range characteristic of the vibrational energies of the molecules. The strong enhancement of the electromagnetic field in the gap region should then lead to an efficient resonant coupling between the plasmon field and the IR active molecular vibrations, and to the visible changes in the optical response of the compound system as compared to that of the nanoantenna alone.[37,38] Eventually, it could allow for the detection of the molecules at low concentration. The quantitative estimate of this sought detection possibility is at the focus of our work.

Molecular detection

IR active vibration. Dipolar coupling

In order to quantify the effect of the plasmon-vibrational coupling we study the absorption spectra of graphene nanoantennas in the presence of CO and N_2 molecules. We start our discussion with an example of the polar CO molecule which has an IR active stretching mode. For the IR active vibration, the molecular dipole depends on the bond length ξ. Therefore, within the classical picture the vibrational excitation can be associated with the dipole oscillating at the transition frequency $\Omega = E_{v=1} - E_{v=0}$. Here E_v stands for the energies of the molecular vibrational states. When a molecule with an IR active vibrational

mode is introduced in the gap of graphene dimer, the oscillating transition dipole couples via the near field with plasmon modes of the nanoantenna rendering the vibrational excitation possible. The $v = 1 \leftarrow 0$ transition can be maximized with a proper choice of E_F so that the BDP of nanoantenna appears resonant with Ω. For the CO molecule with excitation energy $\Omega = 263$ meV (2121.2 cm^{-1}),[72] and consistent with the antenna characteristics reported in Table 1, we use $E_F = 0.36$ eV for the circular dimer and $E_F = 0.40$ eV for the bow-tie antenna.

Within the quantum description: (i) considering the potential energy of the CO dipole, $P_{\mathrm{CO}}(\xi)$, interacting with the plasmon field E_x in the gap, $V = -E_x P_{\mathrm{CO}}(\xi)$, and (ii) developing the molecular dipole in Taylor series in vibrational coordinate ξ around the equilibrium position $\xi = 0$, results in the coupling matrix elements $\mu = \frac{dP_{\mathrm{CO}}(0)}{d\xi} \langle \varphi_{v=0}(\xi)|\xi|\varphi_{v=1}(\xi)\rangle$. The matrix elements μ describe the field induced transition between the molecular vibrational states $\varphi_v(\xi)$. Given the value of μ calculated here ab initio using the quantum chemistry software,[73] we define the molecular polarizability

$$\overleftrightarrow{\alpha}_{\mathrm{Mol}}(\omega) = \hat{e}_M \left[\frac{2\Omega|\mu|^2}{\Omega^2 - \omega^2 - i\omega\eta} \right] \hat{e}_M, \tag{1}$$

which is used together with TDTB inputs to describe the optical absorption of the nanoantenna + CO molecule system, as explained in the Supporting Information. In Eq. 1, $\hat{e}_M$ is the unit length vector along the molecular axis, and η stands for the broadening of molecular line. For the sake of discussion, we first consider the CO molecules located in the gap of graphene dimer with molecular bond aligned along the dimer axis. Since the molecular dipole is collinear with the electric field of the plasmon mode, this geometry is the most efficient for vibrational excitation. The 3D orientation effect will be addressed below in this section.

In Figure 3 we show the absorption spectra of the system where a single CO molecule is localized in the middle of the gap of the circular dimer (panel a) and bow-tie (panel b)

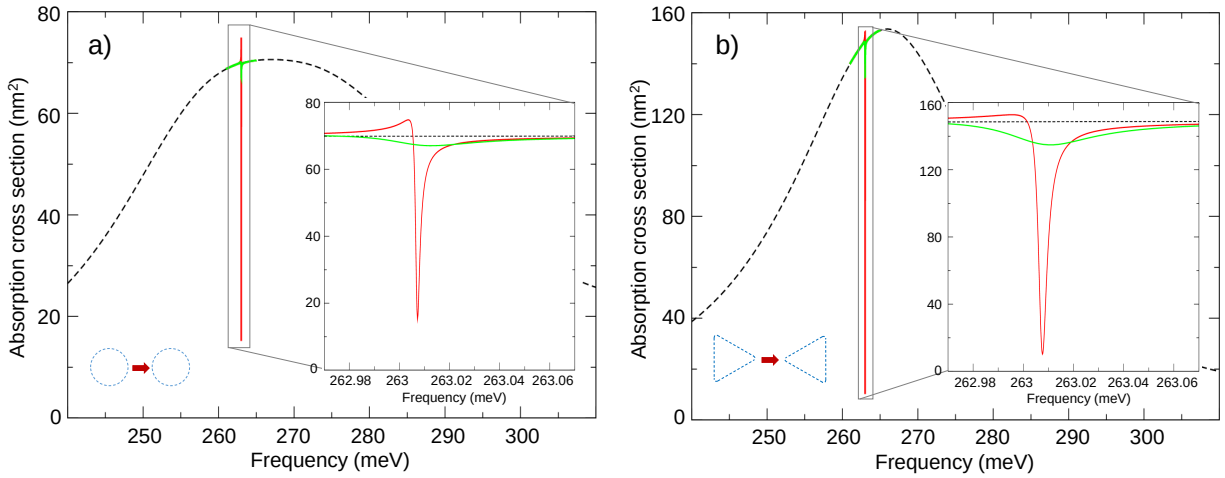

Figure 3: Absorption spectra of the a) circular dimer and b) bow-tie dimer antennas with CO molecule located in the middle of the gap as sketched in the inserts. The molecular bond is oriented along the dimer axis (x-axis). Results are shown as a function of the frequency ω of the electromagnetic x-polarized incident plane wave. Large scale variation of ω reveals the antenna resonance. The inserts zoom into the frequency range close to the vibrational excitation (note that the transition frequency of the isolated CO is 263.014 meV.) The TDTB calculations are performed for the graphene Fermi level energies $E_F = 0.36$ eV (circular geometry) and $E_F = 0.4$ eV (triangular geometry). Dashed black line: the absorption spectra of the nanoantenna; red line: the absorption spectra of the nanoantenna + CO system for the case of the natural broadening of the $v = 1 \leftarrow 0$ transition, $\eta = 2 \times 10^{-14}$ eV;[74] green line: the absorption spectra of the nanoantenna + CO calculated considering $\eta = 0.04$ meV.

graphene nanoantenna. When the plasmon of the nanoantenna is resonant with molecular vibrational excitation, the presence of the CO molecule leads to the enhanced transparency of the system.[42–48,55–57,75–77] Within the narrow frequency range close to the $\Omega = E_{v=1} - E_{v=0}$ a well-resolved absorption dip with a typical Fano profile[78] appears in the frequency dependence of the absorption cross section. Results are very similar for both nanoantenna geometries albeit the resonant variation of the absorption spectra is somewhat stronger for the bow-tie antenna. This can be linked with stronger field enhancement of the latter and better defined plasmon resonance (see Fig. 1 and Fig. 2).

The increased transparency of the system in the vicinity of the $v = 1 \leftarrow 0$ transition is a consequence of the resonant phase shifts between the dipoles induced on graphene and on the molecule. Indeed, since the nanoantenna resonantly drives the molecular dipole the latter experiences a $-\pi/2$ phase shift with respect to the nanoantenna dipole produced by

the incident field. In turn, the molecular dipole leads to the resonant polarisation of the nanoantenna which then has the $-\pi/2$ phase shift with respect to the molecular dipole, and so the $-\pi$ phase shift with respect to the antenna polarization by the incident field. The two contributions appear with different signs thus reducing the total dipole of the nanoantenna and, consequently, absorption.

In the coupled CO + nanoantenna system, the presence of the nanoantenna leads to an energy shift (Lamb shift) and to an additional broadening (Purcell effect) of the molecular transition. These effects emerge because of the self-interaction terms, where the molecule experiences the field created by the nanoantenna in response to the presence of the oscillating molecular dipole (see Supporting Information). Well studied for excitons in plasmonic environments,[11,79–85] the self-interaction leads in the present situation to the energy shift and reduced lifetime of molecular vibrational excitation,[33,86,87] the latter being analogous to the radiation quenching by metal nanostructures.[88–90] It follows from our results that the interplay between the width η of the vibrational transition and the self-interaction induced broadening strongly affects the resonant variation of the absorption spectra.

When η is given by the natural width it is negligibly small compared to the self-interaction induced broadening which then determines the width of the molecular induced feature in the absorption spectra. In this situation, the presence of CO molecule reduces the absorption by up to 10 times at vibrational excitation resonance (red lines in Fig. 3). Notice that the broadening of molecular transition is larger in the case of the bow-tie antenna owing to its stronger field enhancement at the molecule position. Along with absorption spectra calculated for the natural width of the vibrational transition, we also show in Fig. 3 results obtained considering $\eta = 0.04$ meV (0.3 cm^{-1}). This width is measured for CO molecules adsorbed on NaCl,[91,92] and represents here the broadening effects owing to a molecular environment not accounted for by the self-interaction. When $\eta = 0.04$ meV, it overrides the self-interaction term, and determines the width of the Fano profile. The broadening of the molecule transition leads to a smaller resonant variation of the absorption cross section.

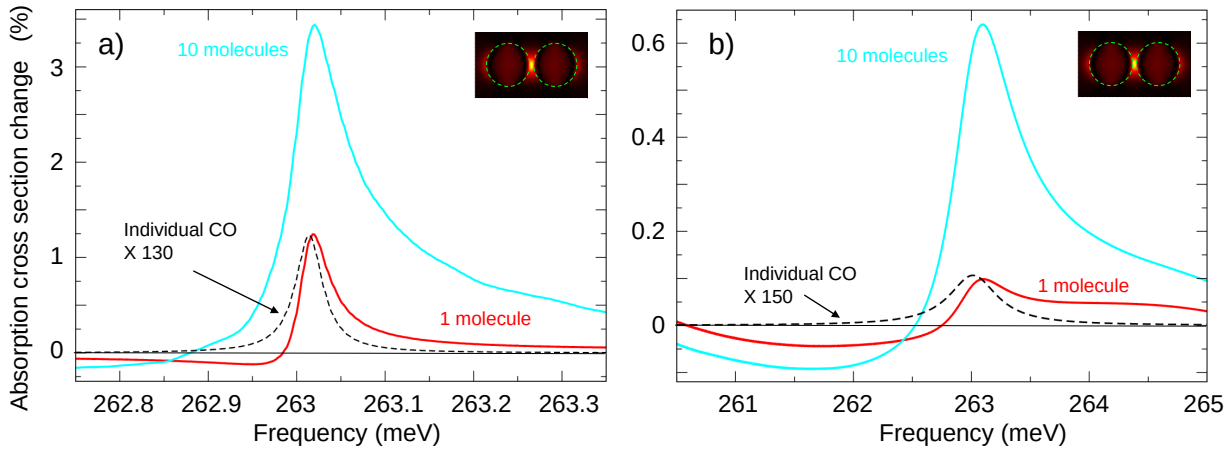

Figure 4: Relative change of the absorption spectra of the circular dimer antenna with plasmonic gap functionalised by the single CO molecule (red lines) and by 10 CO molecules (cyan lines). $E_F = 0.36$ eV. The quantity $\left(\sigma(\omega) - \sigma_{Gr+CO}(\omega)\right)/\sigma(\Omega)$ is shown as function of frequency of the incident x-polarised plane wave. Here $\sigma(\omega)$ is the absorption cross section of the free-standing nanoantenna, $\sigma_{Gr+CO}(\omega)$ is the absorption cross section of the functionalised nanoantenna, and $\sigma(\Omega) = 68$ nm^2 is the absorption cross section of the free-standing nanoantenna at the frequency of vibrational transition. For the single CO molecule, the results are averaged over possible orientations of the molecular bond in 3D space. For the case of the 10 CO molecules, the positions of the molecules are randomly chosen within a rectangle (-0.5 nm $\leq x \leq 0.5$ nm, -1 nm $\leq y \leq 1$ nm, $z = 0$) centered at the gap middle, and molecular orientations are randomly chosen in the 3D space. The absorption spectra shown with cyan lines correspond to an average over 10^3 of such random samples. Panel a: calculations are performed for the molecular line broadening $\eta = 0.04$ meV (0.3 cm^{-1}). Panel b: $\eta = 0.5$ meV (4 cm^{-1}). Dashed black line: normalized absorption cross section of the individual CO molecule in free space $\sigma_{CO}(\omega)/\sigma(\Omega)$.

In order to further explore the sensitivity of the graphene dimer to the presence of CO molecules in the gap, we calculated the optical absorption (i) considering different orientations of the molecular axis, (ii) varying the number of molecules, and (iii) considering $\eta = 0.04$ meV (0.3 cm^{-1}) characteristic for CO absorption on NaCl,[91,92] and $\eta = 0.5$ meV (4 cm^{-1}) characteristic for CO molecules adsorbed on metal surface and strongly coupled with electron and phonon bath.[93,94] Since similar results are obtained in Figure 3 for both antenna geometries, we focus our discussion here on the circular dimer case. Leading to somewhat lower field enhancement as compared to the bow-tie antenna, the circular dimer allows essentially larger spatial extension of enhanced fields which is a clear advantage as far

as molecular detection is concerned.

In Fig. 4 we show the relative change of the absorption cross-section for the situations where a single CO molecule (red), and 10 CO molecules (cyan) are located in the gap. For a single CO molecule, the results are averaged over all possible orientations of the CO bond in the 3D space. In the case of the 10 molecules, they are placed at random positions inside the (-0.5 nm $\leq x \leq 0.5$ nm, -1 nm $\leq y \leq 1$ nm, $z = 0$) rectangle centered at the middle of the gap ($x = 0, y = 0, z = 0$). The orientations of the CO bonds are set random as well, and the results are averaged over 10^3 samples. As a reference, the dashed black line on each panel provides orientation averaged absorption cross section of the individual CO molecule which shows that graphene antenna enhances the sensitivity by more than two orders of magnitude. When comparing with absorption cross section obtained for the molecule aligned along the nanoantenna axis (Fig. 3a), the average over different orientations decreases resonant variation of the absorption cross section. However, the molecule induced change of the absorption remains detectable even for the case of the large width of molecular transition $\eta = 0.5$ meV.

When $N = 10$ molecules are present in the gap the molecule induced feature in the absorption spectrum becomes more pronounced. However, the change with respect to the single CO molecule present in the gap depends on η. It is not proportional to N as one would expect for non-interacting molecules. Incidentally, this result is in line with recent publication studying the near-resonant light scattering by a subwavelength ensemble of identical atoms.[95] For $\eta = 0.04$ meV and $N = 10$, the interaction between the dipoles induced on individual CO molecules broadens the molecule induced feature in the absorption spectrum of the functionalized gap. The 3 times gain in the relative change of an absorption cross section is obtained. When large $\eta = 0.5$ meV is used, the intrinsic width of each individual transition is large compared to the effect of the dipole-dipole interactions. The individual contributions sum up without an additional broadening which favors the proportionality between the number of molecules and the strength of the induced feature in the absorption spectrum. Its

amplitude is increased by six times when the number of CO molecules in the gap changes from 1 to 10.

Our results discussed in this section demonstrate that a very small amount of CO molecules located in the hot spots of the dimer nanoantenna leads to a measurable change of the absorption. In fact, the change of the absorption is sensitive to the presence of a single CO molecule. In this latter case, the effect found here for the plasmonic dimer + single molecule system is quantitatively comparable to that reported for molecular layers adsorbed on graphene nanoribbons.[40–42,44–46] This shows potential interest of the dimer antenna geometry for molecular detection.

At this point it is worth to mention that graphene nanostructures with narrow gaps of some nm have been studied experimentally,[96–99] and theoretically.[66,100,101] At the same time, to the best of our knowledge, the graphene dimer antennas with a few nm gaps have not been reported so far. Nonetheless taking into account the fast progress of the fabrication techniques[102–104] we believe that such devices may become available in the future.

Quadrupolar coupling.

The tight confinement of the near fields of graphene nanoantennas implies their high spatial gradient. Consider an IR inactive molecule which possesses an electrical quadrupole moment. The potential energy of a quadrupole in an electric field $\vec{E}$ is given by $V = -\sum_{ij} Q_{ij}\partial_i E_j$,[105] where $i, j = x, y, z$. This leads to the possibility of the vibrational excitation of the molecule via quadrupolar coupling with plasmon modes of the nanoantenna[106–110] (for further details see the Supporting Information). For the vibrationally excited molecule, the field of the point quadrupole oscillating at the $\Omega = E_{v=1} - E_{v=0}$ frequency induces the dipolar polarisation of the nanoantenna and thus affects the absorption cross section of the coupled system.

In order to have a quantitative measure of the effect and thus of the possibility of the detection of nonpolar molecules, we study the N_2 molecule interacting with graphene nanoantennas. The electrostatic doping of graphene is such that the dipolar plasmon of the nanoan-

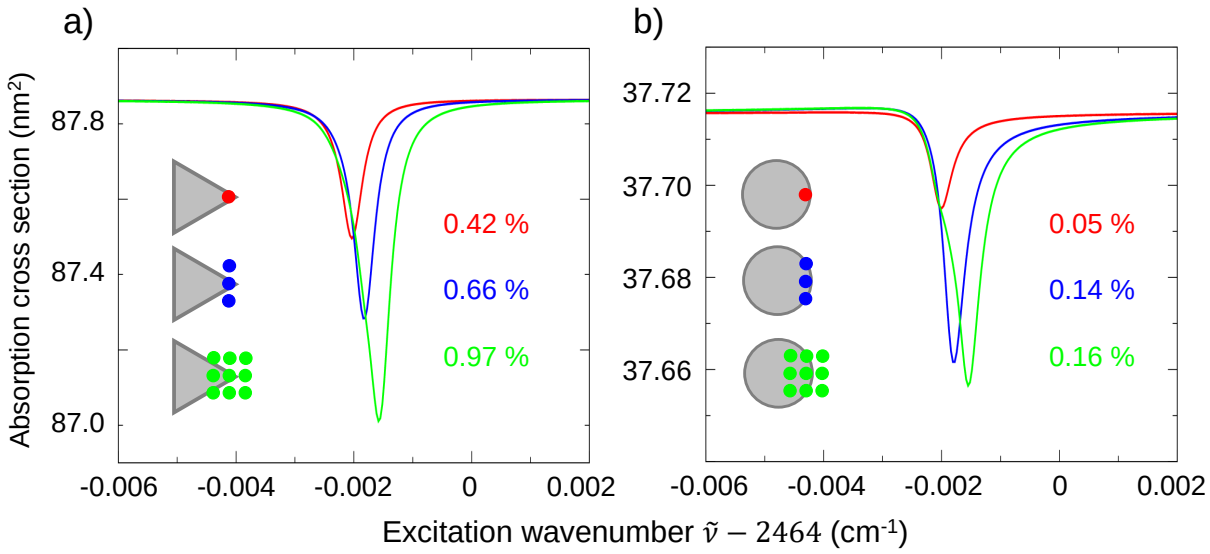

Figure 5: Absorption cross section calculated for triangular (panel a) and circular (panel b) graphene patch antennas functionalized with 1 (red line), 3 (blue line), and 9 (green line) N_2 molecules. The molecules are placed above the edge of the nanoantenna, in the ($z = 1$ nm) plane parallel to the graphene surface. The geometry is sketched in the inserts. The molecular bond is parallel to z-axis. The central molecule is placed just above the hot spot of the nanoantenna (see bottom row of Fig.1). For the case of 3 and 9 molecules the molecule-molecule distance of 1 nm is used. Results are shown as a function of the detuning between the excitation wavenumber and the $v = 1 \leftarrow 0$ transition frequency in the free molecule. The number of the corresponding color gives the amplitude of the relative change of the absorption cross section $(\sigma - \sigma_{N_2})/\sigma$. Here, σ_{N_2} is the absorption cross section of the antenna functionalized with a given number of N_2 molecules, and σ is the absorption cross section of the individual nanoantenna. Both values are taken at vibrational excitation resonance. The electron doping corresponds to $E_F = 0.46$ eV (triangular nanoantenna), and $E_F = 0.40$ eV (circular nanoantenna).

tenna is resonant with transition frequency $\Omega = 296$ meV calculated here using the quantum chemistry software.[73] In contrast with the polar CO molecule studied above, our calculations show that for the quadrupolar coupling the dimer geometry does not allow to enhance the effect of vibrational excitation. Indeed, the field in the gap region is homogeneous while high gradients of the near fields are required for this mechanism of vibrational excitation. These high gradients of the near fields are reached close to the edges of the nanoflakes so that, as compared to the monomer, the dimer antenna simply proposes twice more "hot spots" active for the quadrupolar excitation. Thus, without loss of generality, we will focus our discussion on the results obtained for the monomer nanoantennas of triangular and circular geometry.

The absorption cross sections calculated for the graphene patch antennas of triangular and circular shapes functionalized with N_2 molecules are shown in Fig. 5. The molecules are placed above the edge of the nanoantenna, in the ($z = 1$ nm) plane parallel to graphene surface (see the inserts). The molecular bond is along the z-axis. We found that different molecular orientations lead to similar results. Chosen geometry corresponds to the positioning of the central molecule in the "hot spot" with the largest gradient of the plasmonic near field. It leads to the most sizable effect of molecular presence on the IR absorption. The calculations are performed with $E_F = 0.4$ eV for the triangular nanoantenna, and with $E_F = 0.36$ eV for the circular nanoantenna.

It follows from our results that the absorption cross section of the system shows a clear resonant signature of the N_2 vibrational excitation. The spatially localized "hot spot" plays a dominant role in vibrational excitation. In this situation, the overall per molecule efficiency of the plasmon-vibration coupling is reduced with increasing number of molecules. Indeed, the molecular layer extends out of the "hot spot" region.

In closing this section, one remark is in order regarding the possibility to detect the vibrational excitation of the IR inactive molecules. The calculated N_2 induced feature in the absorption spectra is essentially narrower than that obtained for the CO molecule. This is because the quadrupolar intra-molecule interactions and the self-energy terms are small compared to the dipolar couplings, and the natural width of the transition is negligible. Nonetheless, the narrow absorption dip associated with the N_2 vibrational excitation should be detectable with present experimental capacities.[111] This said, if an additional decay/dephasing mechanisms broaden the molecular line above 10^{-2} meV (0.1 cm^{-1}), the spectral features shown in Fig.5 will become $\approx 10^2$ times smaller rendering the molecular detection impossible even in the case of 9 molecules.

Conclusions and outlook

In conclusion, using (i) the tight binding modeling of the electronic structure of graphene; (ii) the time-dependent quantum calculations of the time evolution of the electron density of graphene nanoantenna in response to an external perturbation; (iii) the quantum chemistry calculations of molecular structure and vibrational states, we addressed the vibrational excitation of molecular species interacting with graphene nanoantenna. We considered circular and triangular shape nanoflakes and their dimers.

Our results demonstrate that graphene nanoantennas allow for enhancement of the vibrational excitation of the molecules located in their vicinity. This is possible owing to the coupling between the plasmonic near field of the nanoantenna and the molecular dipole (for the IR active vibrational modes such as the CO stretch), or molecular quadrupole (discussed here with the example of N_2). When set resonant with the nanoantenna plasmon via charge doping of graphene, the vibrational excitation is particularly efficient for the IR active modes in the case of the molecules located in the gap of the dimer antenna. The molecular signature appears as a narrow Fano-feature in the absorption spectrum with resonantly reduced IR absorption of the nanoantenna + molecule system close to the vibrational transition frequency. This molecular signature persists even considering a strong broadening of the molecular vibrational line as would exist for e.g. metal surface supported molecules. Present results demonstrate that a single CO molecule can be thus detected with some % change of the absorption spectra at the $v = 1 \leftarrow 0$ transition, i.e. we obtain the sensitivity similar to that reported for molecular layers interacting with extended graphene systems such as graphene ribbons.

For the IR inactive molecules, the inhomogeneity of the near fields of the nanoantenna allows the coupling between vibrational excitation and plasmon via molecular quadrupole. With an example of the N_2 molecule we show that $v = 1 \leftarrow 0$ transition leads to an absorption dip in the calculated IR optical response. Quantitatively the effect is essentially smaller than in the case of the CO molecule, and its experimental observation could be difficult in the

situations where the molecular transition is broadened by the environment. It is noteworthy that, in difference with IR active vibrations, the quadrupolar interaction does not require large amplitude of the near field, but rather its high gradient. This places the "hot spots" for vibrational excitation close to the edges of graphene nanoflakes, and the dimer geometry does not perform better than the monomer.

As a final remark, the broadening of the vibrational feature in the absorption spectra results from molecular self-interaction mediated by the nanoantenna. For quantum emitters in metal plasmonic environments, this is the well-known mechanism of the photon-emission quenching near metal nanostructures. In the present case, the broadening of the molecular resonance in absorption reflects the quenching of molecular vibrational excitation via the energy transfer to the electronic excitations in graphene. The possibility of controllable tuning of the lifetimes of vibrational transitions in molecules via electrostatic doping of nearby graphene nanostructures might have implications for photochemistry and single IR photon sources.

We believe that the quantitative character of our analysis is of importance for the development of molecular detection and spectroscopy based on graphene nanostructures since complexity of the nanofabrication techniques invites for theoretical prediction.

Supporting Information Available

The following files are available free of charge. Supporting information providing details on the

- Time dependent tight binding approach to the density dynamics in graphene;
- Calculation of the ground state and of the optical response of the graphene nanoantennas;
- Calculation of the optical response of the nanoantennas functionalised with CO and N_2 molecules.

References

(1) Kauranen, M.; Zayats, A. V. Nonlinear plasmonics. *Nature Photonics* **2012**, *6*, 737–748.

(2) Schoetz, J.; Wang, Z.; Pisanty, E.; Lewenstein, M.; Kling, M. F.; Ciappina, M. F. Perspective on Petahertz Electronics and Attosecond Nanoscopy. *ACS Photonics* **2019**, *6*, 3057–3069.

(3) Nie, S.; Emory, S. R. Probing single molecules and single nanoparticles by Surface-Enhanced Raman Scattering. *Science* **1997**, *275*, 1102–1106.

(4) Mayer, K. M.; Hafner, J. H. Localized surface plasmon resonance sensors. *Chem. Rev.* **2011**, *111*, 3828–3857.

(5) Stewart, M. E.; Anderton, C. R.; Thompson, L. B.; Maria, J.; Gray, S. K.; Rogers, J. A.; Nuzzo, R. G. Nanostructured Plasmonic Sensors. *Chemical Reviews* **2008**, *108*, 494–521.

(6) Langer, J.; Novikov, S. M.; Liz-Marzán, L. M. Sensing using plasmonic nanostructures and nanoparticles. *Nanotechnology* **2015**, *26*, 322001.

(7) Novotny, L.; van Hulst, N. Antennas for light. *Nature Photonics* **2011**, *5*, 83–90.

(8) Törmä, P.; Barnes, W. L. Strong coupling between surface plasmon polaritons and emitters: a review. *Reports on Progress in Physics* **2014**, *78*, 013901.

(9) Koenderink, A. F. Single-Photon Nanoantennas. *ACS Photonics* **2017**, *4*, 710–722.

(10) Vasa, P.; Lienau, C. Strong light - matter interaction in quantum emitter/metal hybrid nanostructures. *ACS Photonics* **2018**, *5*, 2–23.

(11) Carminati, R.; Cazé, A.; Cao, D.; Peragut, F.; Krachmalnicoff, V.; Pierrat, R.; Wilde, Y. D. Electromagnetic density of states in complex plasmonic systems. *Sur. Sci. Rep.* **2015**, *70*, 1–41.

(12) Haran, G.; Chuntonov, L. Artificial plasmonic molecules and their interaction with real molecules. *Chem. Rev.* **2018**, *118*, 5539–5580.

(13) Taminiau, T. H.; Stefani, F. D.; Segerink, F. B.; van Hulst, N. F. Optical antennas direct single-molecule emission. *Nature Photonics* **2008**, *2*, 234–237.

(14) Kaminska, I.; Vietz, C.; Cuartero-González, A.; Tinnefeld, P.; Fernández-Domínguez, A. I.; Acuna, G. P. Strong plasmonic enhancement of single molecule photostability in silver dimer optical antennas. *Nanophotonics* **2018**, *7*, 643–649.

(15) Leon, C. C.; Gunnarsson, O.; de Oteyza, D. G.; Rosławska, A.; Merino, P.; Grewal, A.; Kuhnke, K.; Kern, K. Single Photon Emission from a Plasmonic Light Source Driven by a Local Field-Induced Coulomb Blockade. *ACS Nano* **2020**, *14*, 4216–4223.

(16) Barbry, M.; Koval, P.; Marchesin, F.; Esteban, R.; Borisov, A. G.; Aizpurua, J.; Sánchez-Portal, D. Atomistic near-field nanoplasmonics: reaching atomic-scale resolution in nanooptics. *Nano Lett.* **2015**, *15*, 3410–3419.

(17) Liu, P.; Chulhai, D. V.; Jensen, L. Single-Molecule Imaging Using Atomistic Near-Field Tip-Enhanced Raman Spectroscopy. *ACS Nano* **2017**, *11*, 5094–5102.

(18) Chen, X.; Liu, P.; Hu, Z.; Jensen, L. High-resolution tip-enhanced Raman scattering probes sub-molecular density changes. *Nature Communications* **2019**, *10*, 2567.

(19) Chen, C.; Chu, P.; Bobisch, C. A.; Mills, D. L.; Ho, W. Viewing the interior of a single molecule: vibronically resolved photon imaging at submolecular resolution. *Phys. Rev. Lett.* **2010**, *105*, 217402.

(20) Doppagne, B.; Chong, M. C.; Bulou, H.; Boeglin, A.; Scheurer, F.; Schull, G. Electrofluorochromism at the single-molecule level. *Science* **2018**, *361*, 251–255.

(21) Doppagne, B.; Chong, M. C.; Lorchat, E.; Berciaud, S.; Romeo, M.; Bulou, H.; Boeglin, A.; Scheurer, F.; Schull, G. Vibronic spectroscopy with submolecular resolution from STM-induced electroluminescence. *Phys. Rev. Lett.* **2017**, *118*, 127401.

(22) Imada, H.; Miwa, K.; Imai-Imada, M.; Kawahara, S.; Kimura, K.; Kim, Y. Single-molecule investigation of energy dynamics in a coupled plasmon-exciton system. *Phys. Rev. Lett.* **2017**, *119*, 013901.

(23) Zhang, L.; Yu, Y.-J.; Chen, L.-G.; Luo, Y.; Yang, B.; Kong, F.-F.; Chen, G.; Zhang, Y.; Zhang, Q.; Luo, Y.; Yang, J.-L.; Dong, Z.-C.; Hou, J. G. Electrically driven single-photon emission from an isolated single molecule. *Nat. Commun.* **2017**, *8*, 580.

(24) Rossel, F.; Pivetta, M.; Schneider, W.-D. Luminescence experiments on supported molecules with the scanning tunneling microscope. *Surf. Sci. Rep.* **2010**, *65*, 129–144.

(25) Kuhnke, K.; Große, C.; Merino, P.; Kern, K. Atomic-scale imaging and spectroscopy of electroluminescence at molecular interfaces. *Chem. Rev.* **2017**, *117*, 5174–5222.

(26) Yang, B.; Chen, G.; Ghafoor, A.; Zhang, Y.; Zhang, Y.; Zhang, Y.; Luo, Y.; Yang, J.; Sandoghdar, V.; Aizpurua, J.; Dong, Z.; Hou, J. G. Sub-nanometre resolution in single-molecule photoluminescence imaging. *Nature Photonics* **2020**,

(27) Zhang, R.; Zhang, Y.; Dong, Z. C.; Jiang, S.; Zhang, C.; Chen, L. G.; Zhang, L.; Liao, Y.; Aizpurua, J.; Luo, Y.; Yang, J. L.; Hou, J. G. Chemical mapping of a single molecule by plasmon-enhanced Raman scattering. *Nature* **2013**, *498*, 82.

(28) Jiang, S.; Zhang, Y.; Zhang, R.; Hu, C.; Liao, M.; Luo, Y.; Yang, J.; Dong, Z.; Hou, J. G. Distinguishing adjacent molecules on a surface using plasmon-enhanced Raman scattering. *Nat. Nanotechnol.* **2015**, *10*, 865.

(29) Chiang, N.; Chen, X.; Goubert, G.; Chulhai, D. V.; Chen, X.; Pozzi, E. A.; Jiang, N.; Hersam, M. C.; Seideman, T.; Jensen, L.; Van Duyne, R. P. Conformational contrast of surface - mediated molecular switches yields angstrom-scale spatial resolution in ultrahigh vacuum tip-enhanced Raman spectroscopy. *Nano Lett.* **2016**, *16*, 7774–7778.

(30) Tallarida, N.; Lee, J.; Apkarian, V. A. Tip-enhanced raman Spectromicroscopy on the angstrom scale: bare and CO-terminated Ag tips. *ACS Nano* **2017**, *11*, 11393–11401.

(31) Ebbesen, T. W. Hybrid Light–Matter States in a Molecular and Material Science Perspective. *Accounts of Chemical Research* **2016**, *49*, 2403–2412.

(32) Feist, J.; Galego, J.; Garcia-Vidal, F. J. Polaritonic chemistry with organic molecules. *ACS Photonics* **2018**, *5*, 205–216.

(33) Thomas, A.; Lethuillier-Karl, L.; Nagarajan, K.; Vergauwe, R. M. A.; George, J.; Chervy, T.; Shalabney, A.; Devaux, E.; Genet, C.; Moran, J.; Ebbesen, T. W. Tilting a ground-state reactivity landscape by vibrational strong coupling. *Science* **2019**, *363*, 615–619.

(34) Schedin, F.; Geim, A. K.; Morozov, S. V.; Hill, E. W.; Blake, P.; Katsnelson, M. I.; Novoselov, K. S. Detection of individual gas molecules adsorbed on graphene. *Nature Materials* **2007**, *6*, 652–655.

(35) Sun, J.; Muruganathan, M.; Mizuta, H. Room temperature detection of individual molecular physisorption using suspended bilayer graphene. *Science Advances* **2016**, *2*.

(36) Liu, X.; Ma, T.; Pinna, N.; Zhang, J. Two-Dimensional Nanostructured Materials for Gas Sensing. *Advanced Functional Materials* **2017**, *27*, 1702168.

(37) Yang, X.; Sun, Z.; Low, T.; Hu, H.; Guo, X.; García de Abajo, F. J.; Avouris, P.;

Dai, Q. Nanomaterial-Based Plasmon-Enhanced Infrared Spectroscopy. *Advanced Materials* **2018**, *30*, 1704896.

(38) Taylor, A. B.; Zijlstra, P. Single-Molecule Plasmon Sensing: Current Status and Future Prospects. *ACS Sensors* **2017**, *2*, 1103–1122.

(39) Autore, M.; Li, P.; Dolado, I.; Alfaro-Mozaz, F. J.; Esteban, R.; Atxabal, A.; Casanova, F.; Hueso, L. E.; Alonso-González, P.; Aizpurua, J.; Nikitin, A. Y.; Vélez, S.; Hillenbrand, R. Boron nitride nanoresonators for phonon-enhanced molecular vibrational spectroscopy at the strong coupling limit. *Light: Science and Applications* **2018**, *7*, 17172.

(40) Liu, F.; Cubukcu, E. Tunable omnidirectional strong light-matter interactions mediated by graphene surface plasmons. *Phys. Rev. B* **2013**, *88*, 115439.

(41) Li, Y.; Yan, H.; Farmer, D. B.; Meng, X.; Zhu, W.; Osgood, R. M.; Heinz, T. F.; Avouris, P. Graphene Plasmon Enhanced Vibrational Sensing of Surface-Adsorbed Layers. *Nano Letters* **2014**, *14*, 1573–1577.

(42) Rodrigo, D.; Limaj, O.; Janner, D.; Etezadi, D.; García de Abajo, F. J.; Pruneri, V.; Altug, H. Mid-infrared plasmonic biosensing with graphene. *Science* **2015**, *349*, 165–168.

(43) Farmer, D. B.; Avouris, P.; Li, Y.; Heinz, T. F.; Han, S.-J. Ultrasensitive Plasmonic Detection of Molecules with Graphene. *ACS Photonics* **2016**, *3*, 553–557.

(44) Hu, H.; Yang, X.; Zhai, F.; Hu, D.; Liu, R.; Liu, K.; Sun, Z.; Dai, Q. Far-field nanoscale infrared spectroscopy of vibrational fingerprints of molecules with graphene plasmons. *Nature Communications* **2016**, *7*, 12334.

(45) Hu, H.; Yang, X.; Guo, X.; Khaliji, K.; Romen Biswas, S.; García de Abajo, F. J.;

Low, T.; Sun, Z.; Dai, Q. Gas identification with graphene plasmons. *Nature Communications* **2019**, *10*, 1131.

(46) Khaliji, K.; Biswas, S. R.; Hu, H.; Yang, X.; Dai, Q.; Oh, S.-H.; Avouris, P.; Low, T. Plasmonic Gas Sensing with Graphene Nanoribbons. *Phys. Rev. Applied* **2020**, *13*, 011002.

(47) Marini, A.; Silveiro, I.; García de Abajo, F. J. Molecular Sensing with Tunable Graphene Plasmons. *ACS Photonics* **2015**, *2*, 876–882.

(48) Chen, S.; Autore, M.; Li, J.; Li, P.; Alonso-Gonzalez, P.; Yang, Z.; Martin-Moreno, L.; Hillenbrand, R.; Nikitin, A. Y. Acoustic Graphene Plasmon Nanoresonators for Field-Enhanced Infrared Molecular Spectroscopy. *ACS Photonics* **2017**, *4*, 3089–3097.

(49) Zundel, L.; Manjavacas, A. Spatially Resolved Optical Sensing Using Graphene Nanodisk Arrays. *ACS Photonics* **2017**, *4*, 1831–1838.

(50) Yu, R.; Cox, J. D.; de Abajo, F. J. G. Nonlinear Plasmonic Sensing with Nanographene. *Phys. Rev. Lett.* **2016**, *117*, 123904.

(51) Belacel, C.; Habert, B.; Bigourdan, F.; Marquier, F.; Hugonin, J.-P.; Michaelis de Vasconcellos, S.; Lafosse, X.; Coolen, L.; Schwob, C.; Javaux, C.; Dubertret, B.; Greffet, J.-J.; Senellart, P.; Maitre, A. Controlling spontaneous emission with plasmonic optical patch antennas. *Nano Lett.* **2013**, *13*, 1516–1521.

(52) Chikkaraddy, R.; de Nijs, B.; Benz, F.; Barrow, S. J.; Scherman, O. A.; Rosta, E.; Demetriadou, A.; Fox, P.; Baumberg, J. J. Single-molecule strong coupling at room temperature in plasmonic nanocavities. *Nature* **2016**, *535*, 127.

(53) Benz, F.; Schmidt, M. K.; Dreismann, A.; Chikkaraddy, R.; Zhang, Y.; Demetriadou, A.; Carnegie, C.; Ohadi, H.; de Nijs, B.; Esteban, R.; Aizpurua, J.; Baumberg, J. J. Single-molecule optomechanics in picocavities. *Science* **2016**, *354*, 726–729.

(54) Sun, J.; Hu, H.; Zheng, D.; Zhang, D.; Deng, Q.; Zhang, S.; Xu, H. Light - emitting plexciton: exploiting plasmon - exciton interaction in the intermediate coupling regime. *ACS Nano* **2018**, *12*, 10393–10402.

(55) Schlather, A. E.; Large, N.; Urban, A. S.; Nordlander, P.; Halas, N. J. Near-Field Mediated Plexcitonic Coupling and Giant Rabi Splitting in Individual Metallic Dimers. *Nano Letters* **2013**, *13*, 3281–3286.

(56) Savasta, S.; Saija, R.; Ridolfo, A.; Di Stefano, O.; Denti, P.; Borghese, F. Nanopolaritons: Vacuum Rabi Splitting with a Single Quantum Dot in the Center of a Dimer Nanoantenna. *ACS Nano* **2010**, *4*, 6369–6376.

(57) Manjavacas, A.; García de Abajo, F. J.; Nordlander, P. Quantum plexcitonics: strongly interacting plasmons and excitons. *Nano Lett.* **2011**, *11*, 2318–2323.

(58) Kinkhabwala, A.; Yu, Z.; Fan, S.; Avlasevich, Y.; Müllen, K.; Moerner, W. E. Large single-molecule fluorescence enhancements produced by a bowtie nanoantenna. *Nature Photonics* **2009**, *3*, 654–657.

(59) Wang, H.; Brandl, D. W.; Nordlander, P.; Halas, N. J. Plasmonic Nanostructures: Artificial Molecules. *Accounts of Chemical Research* **2007**, *40*, 53–62.

(60) Thongrattanasiri, S.; Manjavacas, A.; García de Abajo, F. J. Quantum Finite-Size Effects in Graphene Plasmons. *ACS Nano* **2012**, *6*, 1766–1775.

(61) Cox, J. D.; Silveiro, I.; García de Abajo, F. J. Quantum Effects in the Nonlinear Response of Graphene Plasmons. *ACS Nano* **2016**, *10*, 1995–2003.

(62) Romero, I.; Aizpurua, J.; Bryant, G. W.; de Abajo, F. J. G. Plasmons in nearly touching metallic nanoparticles: singular response in the limit of touching dimers. *Opt. Express* **2006**, *14*, 9988–9999.

(63) Zuloaga, J.; Prodan, E.; Nordlander, P. Quantum description of the plasmon resonances of a nanoparticle dimer. *Nano Lett.* **2009**, *9*, 887–891.

(64) Marinica, D.; Kazansky, A.; Nordlander, P.; Aizpurua, J.; Borisov, A. G. Quantum plasmonics: Nonlinear effects in the field enhancement of a plasmonic nanoparticle dimer. *Nano Lett.* **2012**, *12*, 1333–1339.

(65) Varas, A.; García-González, P.; Feist, J.; García-Vidal, F.; Rubio, A. Quantum plasmonics: from jellium models to ab initio calculations. *Nanophotonics* **2016**, *5*, 409–426.

(66) Thongrattanasiri, S.; Manjavacas, A.; Nordlander, P.; de Abajo, F. J. G. Quantum junction plasmons in graphene dimers. *Laser and Photonics Reviews* **2013**, *7*, 297–302.

(67) Thongrattanasiri, S.; García de Abajo, F. J. Optical Field Enhancement by Strong Plasmon Interaction in Graphene Nanostructures. *Phys. Rev. Lett.* **2013**, *110*, 187401.

(68) Wang, W.; Christensen, T.; Jauho, A.-P.; Thygesen, K. S.; Wubs, M.; Mortensen, N. A. Plasmonic eigenmodes in individual and bow-tie graphene nanotriangles. *Scientific Reports* **2015**, *5*, 9535.

(69) Christensen, T.; Wang, W.; Jauho, A.-P.; Wubs, M.; Mortensen, N. A. Classical and quantum plasmonics in graphene nanodisks: Role of edge states. *Phys. Rev. B* **2014**, *90*, 241414.

(70) Jablan, M.; Buljan, H.; Soljačić, M. Plasmonics in graphene at infrared frequencies. *Phys. Rev. B* **2009**, *80*, 245435.

(71) Yu, R.; Cox, J. D.; Saavedra, J. R. M.; García de Abajo, F. J. Analytical Modeling of Graphene Plasmons. *ACS Photonics* **2017**, *4*, 3106–3114.

(72) Langhoff, S. R.; Bauschlicher, C. W. Global dipole moment function for the $X^1\Sigma^+$ ground state of CO. *The Journal of Chemical Physics* **1995**, *102*, 5220–5225.

(73) Frisch, M. J. et al. Gaussian~16 Revision C.01. 2016; Gaussian Inc. Wallingford CT.

(74) Ferguson, M. G.; Read, A. W. Vibrational relaxation of carbon monoxide at room temperature. *Trans. Faraday Soc.* **1965**, *61*, 1559–1563.

(75) Ridolfo, A.; Di Stefano, O.; Fina, N.; Saija, R.; Savasta, S. Quantum Plasmonics with Quantum Dot-Metal Nanoparticle Molecules: Influence of the Fano Effect on Photon Statistics. *Phys. Rev. Lett.* **2010**, *105*, 263601.

(76) Shah, R. A.; Scherer, N. F.; Pelton, M.; Gray, S. K. Ultrafast reversal of a Fano resonance in a plasmon-exciton system. *Phys. Rev. B* **2013**, *88*, 075411.

(77) Hartsfield, T.; Chang, W.-S.; Yang, S.-C.; Ma, T.; Shi, J.; Sun, L.; Shvets, G.; Link, S.; Li, X. Single quantum dot controls a plasmonic cavity's scattering and anisotropy. *Proceedings of the National Academy of Sciences* **2015**, *112*, 12288–12292.

(78) Luk'yanchuk, B.; Zheludev, N. I.; Maier, S. A.; Halas, N. J.; Nordlander, P.; Giessen, H.; Chong, C. T. The Fano resonance in plasmonic nanostructures and metamaterials. *Nature Materials* **2010**, *9*, 707–715.

(79) Bouchet, D.; Carminati, R. Quantum dipole emitters in structured environments: a scattering approach: tutorial. *J. Opt. Soc. Am. A* **2019**, *36*, 186–195.

(80) Li, T. E.; Nitzan, A.; Sukharev, M.; Martinez, T.; Chen, H.-T.; Subotnik, J. E. Mixed quantum-classical electrodynamics: Understanding spontaneous decay and zero-point energy. *Phys. Rev. A* **2018**, *97*, 032105.

(81) Andreussi, O.; Corni, S.; Mennucci, B.; Tomasi, J. Radiative and nonradiative decay rates of a molecule close to a metal particle of complex shape. *J. Chem. Phys.* **2004**, *121*, 10190–10202.

(82) Akselrod, G. M.; Argyropoulos, C.; Hoang, T. B.; Ciracì, C.; Fang, C.; Huang, J.;

Smith, D. R.; Mikkelsen, M. H. Probing the mechanisms of large Purcell enhancement in plasmonic nanoantennas. *Nature Photonics* **2014**, *8*, 835.

(83) Zhang, C.; Chen, B.-Q.; Li, Z.-Y. Optical origin of subnanometer resolution in tip-enhanced raman mapping. *J. Phys. Chem. C* **2015**, *119*, 11858–11871.

(84) Aguilar-Galindo, F.; Díaz-Tendero, S.; Borisov, A. G. Electronic Structure Effects in the Coupling of a Single Molecule with a Plasmonic Antenna. *The Journal of Physical Chemistry C* **2019**, *123*, 4446–4456.

(85) Sukharev, M.; Freifeld, N.; Nitzan, A. Numerical calculations of radiative and non-radiative relaxation of molecules near metal particles. *J. Phys. Chem. C* **2014**, *118*, 10545–10551.

(86) Ford, G.; Weber, W. Electromagnetic interactions of molecules with metal surfaces. *Phys. Rep.* **1984**, *113*, 195–287.

(87) Galego, J.; Climent, C.; Garcia-Vidal, F. J.; Feist, J. Cavity Casimir-Polder Forces and Their Effects in Ground-State Chemical Reactivity. *Phys. Rev. X* **2019**, *9*, 021057.

(88) Carminati, R.; Greffet, J.-J.; Henkel, C.; Vigoureux, J. Radiative and non-radiative decay of a single molecule close to a metallic nanoparticle. *Opt. Commun.* **2006**, *261*, 368–375.

(89) Anger, P.; Bharadwaj, P.; Novotny, L. Enhancement and Quenching of Single-Molecule Fluorescence. *Phys. Rev. Lett.* **2006**, *96*, 113002.

(90) Delga, A.; Feist, J.; Bravo-Abad, J.; Garcia-Vidal, F. J. Quantum emitters near a metal nanoparticle: strong coupling and quenching. *Phys. Rev. Lett.* **2014**, *112*, 253601.

(91) Chang, H.-C.; Ewing, G. E. Infrared fluorescence from a monolayer of CO on NaCl(100). *Phys. Rev. Lett.* **1990**, *65*, 2125–2128.

(92) Heidberg, J.; Kampshoff, E.; Kühnemuth, R.; Suhren, M.; Weiss, H. Fourier-transform infrared spectra of CO adsorbed on NaCl(100): structural changes at low temperatures. *Surface Science* **1992**, *269-270*, 128 – 134.

(93) Bonn, M.; Hess, C.; Wolf, M. The dynamics of vibrational excitations on surfaces: CO on Ru(001). *The Journal of Chemical Physics* **2001**, *115*, 7725–7735.

(94) Kumar, S.; Jiang, H.; Schwarzer, M.; Kandratsenka, A.; Schwarzer, D.; Wodtke, A. M. Vibrational Relaxation Lifetime of a Physisorbed Molecule at a Metal Surface. *Phys. Rev. Lett.* **2019**, *123*, 156101.

(95) Schilder, N. J.; Sauvan, C.; Sortais, Y. R. P.; Browaeys, A.; Greffet, J.-J. Near-Resonant Light Scattering by a Subwavelength Ensemble of Identical Atoms. *Phys. Rev. Lett.* **2020**, *124*, 073403.

(96) Ullmann, K.; Coto, P. B.; Leitherer, S.; Molina-Ontoria, A.; Martín, N.; Thoss, M.; Weber, H. B. Single-Molecule Junctions with Epitaxial Graphene Nanoelectrodes. *Nano Letters* **2015**, *15*, 3512–3518.

(97) Puczkarski, P.; Wu, Q.; Sadeghi, H.; Hou, S.; Karimi, A.; Sheng, Y.; Warner, J. H.; Lambert, C. J.; Briggs, G. A. D.; Mol, J. A. Low-Frequency Noise in Graphene Tunnel Junctions. *ACS Nano* **2018**, *12*, 9451–9460.

(98) Ott, C.; Götzinger, S.; Weber, H. B. Thermal origin of light emission in nonresonant and resonant nanojunctions. *Phys. Rev. Research* **2020**, *2*, 042019.

(99) Sarwat, S. G.; Gehring, P.; Rodriguez Hernandez, G.; Warner, J. H.; Briggs, G. A. D.; Mol, J. A.; Bhaskaran, H. Scaling Limits of Graphene Nanoelectrodes. *Nano Letters* **2017**, *17*, 3688–3693, PMID: 28481105.

(100) Christensen, J.; Manjavacas, A.; Thongrattanasiri, S.; Koppens, F. H. L.; García de

Abajo, F. J. Graphene Plasmon Waveguiding and Hybridization in Individual and Paired Nanoribbons. *ACS Nano* **2012**, *6*, 431–440, PMID: 22147667.

(101) Manrique, D. Z.; You, J. W.; Deng, H.; Ye, F.; Panoiu, N. C. Quantum Plasmon Engineering with Interacting Graphene Nanoflakes. *The Journal of Physical Chemistry C* **2017**, *121*, 27597–27602.

(102) Yano, Y.; Mitoma, N.; Ito, H.; Itami, K. A Quest for Structurally Uniform Graphene Nanoribbons: Synthesis, Properties, and Applications. *The Journal of Organic Chemistry* **2020**, *85*, 4–33, PMID: 31789025.

(103) Nef, C.; Pósa, L.; Makk, P.; Fu, W.; Halbritter, A.; Schönenberger, C.; Calame, M. High-yield fabrication of nm-size gaps in monolayer CVD graphene. *Nanoscale* **2014**, *6*, 7249–7254.

(104) Liu, Z.; Ren, S.; Guo, X. Switching Effects in Molecular Electronic Devices. *Topics in Current Chemistry* **2017**, *375*, 56.

(105) Barron, L. D.; Gray, C. G. The multipole interaction Hamiltonian for time dependent fields. *Journal of Physics A: Mathematical, Nuclear and General* **1973**, *6*, 59–61.

(106) Yannopapas, V.; Paspalakis, E. Giant enhancement of dipole-forbidden transitions via lattices of plasmonic nanoparticles. *Journal of Modern Optics* **2015**, *62*, 1435–1441.

(107) Shibata, K.; Tojo, S.; Bloch, D. Excitation enhancement in electric multipole transitions near a nanoedge. *Opt. Express* **2017**, *25*, 9476–9489.

(108) Sanders, S.; May, A.; Alabastri, A.; Manjavacas, A. Extraordinary Enhancement of Quadrupolar Transitions Using Nanostructured Graphene. *ACS Photonics* **2018**, *5*, 3282–3290.

(109) Rusak, E.; Straubel, J.; Gładysz, P.; Göddel, M.; Kedziorski, A.; Kühn, M.; Weigend, F.; Rockstuhl, C.; Słowik, K. Enhancement of and interference among higher

order multipole transitions in molecules near a plasmonic nanoantenna. *Nature Communications* **2019**, *10*, 5775.

(110) Cuartero-González, A.; Fernández-Domínguez, A. I. Dipolar and quadrupolar excitons coupled to a nanoparticle-on-mirror cavity. *Phys. Rev. B* **2020**, *101*, 035403.

(111) Germann, M.; Tong, X.; Willitsch, S. Observation of electric-dipole-forbidden infrared transitions in cold molecular ions. *Nature Physics* **2014**, *10*, 820–824.

Graphical TOC Entry